Title
An investigation of the rare-earth telluride system BaLn2Te4 (Ln=Sm–Tm, Y): syntheses, crystal structures, and magnetic properties

Authors
Narducci, Amy A
Yang, Yuting
Digman, Michelle A
et al.

Publication Date
2000-05-01

DOI
10.1016/s0925-8388(00)00653-8

ELSEVIER

Journal of Alloys and Compounds 303–304 (2000) 432–439

Journal of ALLOYS AND COMPOUNDS

www.elsevier.com/locate/jallcom

An investigation of the rare-earth telluride system $BaLn_2Te_4$ (Ln=Sm–Tm, Y): syntheses, crystal structures, and magnetic properties

Amy A. Narducci, Yuting Yang, Michelle A. Digman, Abe B. Sipes, James A. Ibers*

Department of Chemistry, Northwestern University, 2145 Sheridan Road, Evanston, IL 60208-3113, USA

Abstract

Single crystals of $BaLn_2Te_4$ (Ln=Gd–Tm, Y) form as black needles from the stoichiometric reaction BaTe+2Ln+3Te at 1000°C. $BaSm_2Te_4$ forms as a by-product in the reaction BaTe+Sm+Zn+Te at 850°C with the aid of a $BaBr_2$/KBr flux. The compounds crystallize with four formula units in the space group D_{2h}^{16}–*Pnma* (No. 62) in the $CaFe_2O_4$ (calcium ferrite) structure type. Unit cell constants range from a=13.6883(10) Å, b=4.5148(3) Å, and c=16.3427(12) Å in the Sm compound to a=13.5677(10) Å, b=4.4058(3) Å, and c=15.9989(12) Å for Tm (t=−120°C). Ln atoms are coordinated by six Te atoms in an octahedral arrangement. These octahedra share corners and edges to form a three-dimensional channel structure. Ba atoms occupy the bicapped trigonal-prismatic sites within these channels. Magnetic susceptibility data for two representative compounds (Ln=Er and Tb) show paramagnetic behavior in the region 5–300 K.

Keywords: Synthesis; Solid-state compounds; Tellurides; Rare-earths

1. Introduction

The family of compounds MLn_2Q_4 (M=divalent cation; Ln=La–Lu, Y; Q=O, S, Se) has been discussed in detail in the literature [1–15]. The family comprises a variety of similar structure types with the majority of compounds adopting the Yb_3S_4, MnY_2S_4, Th_3P_4, or $CaFe_2O_4$ (calcium ferrite) structures. In addition to the reaction temperature, the sizes of the M^{2+} and Ln^{3+} cations and Q^{2-} anion determine the structure type adopted by a given compound. Several studies of the MLn_2Q_4 system have mapped these trends [16–18]. However, a large portion of the data used involves powder X-ray diffraction methods as the only form of structural identification and some of these data have been questioned [19–21]. Thus, a complete picture of the structural trends in this system is lacking. Additionally, the behavior of the telluride analogues is virtually unknown, as only a few compounds have been reported [7]. To this end, the compounds $BaLn_2Te_4$ (Ln=Sm–Tm, Y) have been synthesized and structurally characterized. The magnetic properties of two representative compounds have also been studied.

2. Experimental

2.1. Syntheses

Single crystals of $BaLn_2Te_4$ (Ln=Gd–Tm, Y) were synthesized by reacting the appropriate Ln element with BaTe and Te in stoichiometric amounts at 1000°C for 6 days in evacuated fused silica tubes. The reagents used were: Dy, Er (Aldrich 99.9%); Eu, Gd, Ho, Sm, Y (Alfa Aesar 99.9%); Tb, Tm (Strem 99.9%); BaTe (Alfa Aesar 99.5%); and Te (Aldrich 99.8%). The reactions proceeded in good yield, from 40% to 100% (for Er and Tm) of crystals and powder; binary rare-earth tellurides were the major impurities. The purity of bulk powder samples was checked by comparing experimental and calculated X-ray diffraction patterns. For Ln=Sm the stoichiometric procedure failed, but a few single crystals were obtained unexpectedly in the reaction of BaTe, Sm, Zn, and Te in a $BaBr_2$/KBr flux (1.1/1 ratio) at 850°C for 6 days. Single crystals were manually extracted from the product mixtures. The elemental contents of all single crystals used for diffraction studies were determined by means of an EDS-equipped Hitachi-4500 SEM; atomic ratios were found to be approximately Ba:Ln:Te=1:2:4.

All attempts to prepare the analogous compounds of the lighter rare earths (La–Sm) by this stoichiometric route

*Corresponding author. Tel.: +1-847-491-5449.

0925-8388/00/$ – see front matter
PII: S0925-8388(00)00653-8

failed. For Eu, transparent red crystals of nominal composition $BaEu_4Te_5$ were obtained. As Eu is most often divalent in solid-state chalcogenides, we would not expect $BaEu_2Te_4$ to exist as a stable phase.

2.2. Crystallographic details

Small black needles of each compound were used for single-crystal diffraction studies. Each crystal was mounted on the end of a glass fiber and placed in the cold stream [22] of a Bruker SMART-1000 instrument equipped with a CCD detector. The samples were kept at −120°C throughout the data collection. Data were collected with 0.3° ω scans for either 15, 20, or 30 s for each frame depending on the size of each crystal and hence the intensity of its diffraction pattern. Final unit cell parameters were obtained by a global refinement of the positions of all reflections with the use of the processing program SAINT+ [23]. A face-indexed absorption correction was applied to each data set with the use of XPREP [24] and subsequently the program SADABS [23], which relies on redundancy in the data, was used to apply some semi-empirical corrections. Each structure was solved with the use of the direct methods program SHELXS [25] of the SHELXTL-97 suite. The structures were refined by full-matrix, least-squares techniques with the program SHELXL-97 [24]. Final refinements included anisotropic displacement parameters and, for the Sm, Gd, and Tm compounds, secondary extinction corrections. Relevant crystallographic parameters are presented in Table 1. Final positional parameters and equivalent isotropic displacement parameters are given in Table 2.

2.3. Magnetic susceptibility

Samples of $BaEr_2Te_4$ and $BaTm_2Te_4$ weighing approximately 0.150 g were ground into fine powders and used for magnetic susceptibility measurements. The purity of each sample was checked by powder X-ray diffraction methods. Magnetization of each sample was measured as a function of both temperature and field strength with a Quantum Design SQUID magnetometer. All measurements were corrected for core diamagnetism [26]. Plots of magnetization versus field strength at 35 K indicate no hysteresis up to 10^4 G.

3. Results and discussion

The compounds $BaLn_2Te_4$ (Ln=Sm–Tm, Y) crystallize in the calcium ferrite structure type (Fig. 1). The structure consists of two crystallographically unique Ln atoms each coordinated in an octahedral arrangement by six Te atoms, as well as one Ba atom at the center of a bicapped trigonal prism of Te atoms. Each Ln-centered octahedron shares edges to form two distinct dimers, i.e. $Ln(1)_2Te_{10}$ and $Ln(2)_2Te_{10}$, illustrated in the polyhedral view in Fig. 2. Each octahedron of the pair shares edges with octahedra of two neighboring dimers to form infinite one-dimensional chains along [010], ($^1_\infty[Ln(1)_2Te_{10}]$ and $^1_\infty[Ln(2)_2Te_{10}]$). Additionally, each dimer shares corners with four neighboring dimers to form layers perpendicular to [010], creating a three-dimensional channel structure. Ba^{2+} cations fill the bicapped-trigonal prismatic sites within these channels. Selected Ln–Te bond distances (Table 3) agree well with literature values, i.e. 3.1–3.7 Å for Gd_2Te_3 [27] and 3.1–3.3 Å for $(HoS)_2Te_{1.34}$ [28]. The angles (Table 4) of the octahedron surrounding atom Ln(1) are within about 4° of 90° or 180°. The angles of the octahedron around atom Ln(2), however, deviate far more, up to approximately 18°. This distortion of both octahedral sites is inherent in the $CaFe_2O_4$ structure type [29]. The nature and effects of this distortion will be discussed below.

Owing to the large size of the Ba^{2+} cations, it is not surprising that the present compounds form the $CaFe_2O_4$ structure type. The preference of larger divalent cations for the calcium ferrite structure over the related, mixed-valent

Table 1
Crystal data and structure refinement for $BaLn_2Te_4$[a]

Ln=	Sm	Gd	Tb	Dy	Y	Ho	Tm	Er
Formula weight	948.44	962.24	965.58	972.74	825.56	977.60	982.26	985.60
a (Å)	13.6883 (10)	13.6924 (8)	13.6611 (14)	13.6567 (12)	13.646 (3)	13.6211 (9)	13.5992 (12)	13.5677 (10)
b	4.5148 (3)	4.4822 (2)	4.4611 (5)	4.4517 (4)	4.4430 (9)	4.4322 (3)	4.4177 (4)	4.4058 (3)
c	16.3427 (12)	16.2597 (9)	16.1817 (16)	16.1465 (14)	16.141 (3)	16.0959 (11)	16.0487 (14)	15.9989 (12)
Volume (Å^3)	1009.98 (12)	997.89 (9)	986.17 (18)	981.64 (15)	978.6 (3)	971.73 (11)	964.16 (15)	956.36 (12)
ρ (calc.) (g/cm^3)	6.237	6.405	6.503	6.582	5.603	6.682	6.767	6.845
μ (cm^{-1})	266	284	296	306	273	318	331	343
$R(F)$, $F_o^2>2\sigma(F_o^2)$[b]	0.0271	0.0192	0.0337	0.0282	0.0401	0.0230	0.0264	0.0238
$Rw(F^2)$ (all data)[c]	0.0692	0.0581	0.0738	0.0609	0.0863	0.0554	0.0627	0.0519

[a] Space group: *Pnma*, $Z=4$, $t=-120$°C.
[b] $R(F)=\Sigma||F_o|-|F_c||/\Sigma|F_o|$.
[c] $R_w(F_o^2)=[\Sigma w(F_o^2-F_c^2)^2/\Sigma wF_o^4]^{1/2}$; $w^{-1}=\sigma^2(F_o^2)+(pF_o^2)^2$ for $F_o^2\geq 0$; $w^{-1}=\sigma^2(F_o^2)$ for $F_o^2\leq 0$. $p=0.04$ (Sm, Gd, Y); 0.033 (Tb); 0.03 (Dy, Ho, Er); 0.025 (Tm).

Table 2
Atomic coordinates and equivalent isotropic displacement parameters for $BaLn_2Te_4$ ($y=1/4$)

Atom	x	z	U(eq)[a]	Atom	x	z	U(eq)[a]
$BaSm_2Te_4$				*BaY_2Te_4*			
Ba(1)	0.24141(4)	0.66665(3)	0.01187(14)	Ba(1)	0.23889(7)	0.66913(5)	0.0115(2)
Sm(1)	0.07940(3)	0.40225(2)	0.01112(14)	Y(1)	0.08125(11)	0.40353(9)	0.0110(3)
Sm(2)	0.56575(3)	0.60830(2)	0.01147(14)	Y(2)	0.55953(11)	0.60943(9)	0.0108(3)
Te(1)	0.08814(4)	0.07940(3)	0.01083(15)	Te(1)	0.09127(7)	0.07663(6)	0.0101(2)
Te(2)	0.29246(4)	0.33124(3)	0.01146(15)	Te(2)	0.29519(8)	0.33836(6)	0.0110(2)
Te(3)	0.36809(4)	0.02744(3)	0.01082(15)	Te(3)	0.37190(7)	0.02899(6)	0.0104(2)
Te(4)	0.47686(4)	0.78343(3)	0.01167(15)	Te(4)	0.47294(7)	0.78393(6)	0.0108(2)
$BaGd_2Te_4$				*$BaHo_2Te_4$*			
Ba(1)	0.23972(3)	0.66821(3)	0.01013(12)	Ba(1)	0.23871(4)	0.66939(4)	0.00969(13)
Gd(1)	0.08057(2)	0.40311(2)	0.00951(11)	Ho(1)	0.08109(3)	0.40356(3)	0.00906(12)
Gd(2)	0.56224(2)	0.60884(2)	0.00983(11)	Ho(2)	0.55951(3)	0.60933(3)	0.00920(11)
Te(1)	0.09027(3)	0.07807(3)	0.00938(13)	Te(1)	0.09094(4)	0.07659(4)	0.00879(14)
Te(2)	0.29393(3)	0.33492(3)	0.00996(12)	Te(2)	0.29501(5)	0.33924(4)	0.00970(15)
Te(3)	0.37008(3)	0.02855(3)	0.00931(12)	Te(3)	0.37227(5)	0.02883(4)	0.00904(14)
Te(4)	0.47463(3)	0.78376(3)	0.01008(12)	Te(4)	0.47312(5)	0.78407(4)	0.00954(14)
$BaTb_2Te_4$				*$BaEr_2Te_4$*			
Ba(1)	0.23930(7)	0.66866(6)	0.0104(2)	Ba(1)	0.23863(6)	0.66963(5)	0.00951(19)
Tb(1)	0.08077(6)	0.40313(5)	0.00965(19)	Er(1)	0.08120(5)	0.40360(4)	0.00896(15)
Tb(2)	0.56109(6)	0.60890(5)	0.01007(19)	Er(2)	0.55892(5)	0.60941(4)	0.00907(15)
Te(1)	0.09050(8)	0.07753(6)	0.0093(2)	Te(1)	0.09097(6)	0.07626(5)	0.0087(2)
Te(2)	0.29443(8)	0.33680(6)	0.0099(2)	Te(2)	0.29529(7)	0.34039(5)	0.0091(2)
Te(3)	0.37097(8)	0.02864(6)	0.0096(2)	Te(3)	0.37272(7)	0.02881(5)	0.0084(2)
Te(4)	0.47399(8)	0.78392(6)	0.0104(2)	Te(4)	0.47271(7)	0.78413(5)	0.0092(2)
$BaDy_2Te_4$				*$BaTm_2Te_4$*			
Ba(1)	0.23897(6)	0.66910(5)	0.01020(18)	Ba(1)	0.23854(5)	0.66982(4)	0.01043(15)
Dy(1)	0.08101(5)	0.40342(4)	0.00943(15)	Tm(1)	0.08119(3)	0.40357(3)	0.00974(12)
Dy(2)	0.56017(5)	0.60919(4)	0.00978(15)	Tm(2)	0.55870(4)	0.60949(3)	0.00989(12)
Te(1)	0.09085(6)	0.07693(5)	0.00914(19)	Te(1)	0.09087(5)	0.07595(4)	0.00925(15)
Te(2)	0.29468(6)	0.33812(5)	0.0099(2)	Te(2)	0.29532(5)	0.34126(4)	0.01016(16)
Te(3)	0.37180(6)	0.02883(5)	0.00917(19)	Te(3)	0.37329(5)	0.02859(4)	0.00942(16)
Te(4)	0.47338(6)	0.78388(5)	0.01007(19)	Te(4)	0.47266(5)	0.78419(4)	0.01002(16)

[a] U(eq) is defined as one third of the trace of the orthogonalized U_{ij} tensor.

Yb_3Se_4 structure type has been discussed in detail [15]. For example, CaY_2S_4 adopts the Yb_3S_4 structure type consisting of a three-dimensional Ln-centered octahedral framework that accommodates the two small cations in the channels of the structure. SrY_2S_4 and BaY_2S_4, however, form the calcium ferrite structure that can only accommodate one large cation in each channel. The size of the Ln^{3+} cation also plays a role in determining structure type; this can be seen for oxides, sulfides, and selenides, and all M^{2+} cations in the MLn_2Q_4 family. In the Sr and Ba selenides, the larger lanthanides form the Th_3P_4 structure whereas the smaller lanthanides crystallize in the calcium ferrite structure [18]. The structural change occurs between Gd and Tb for the Sr compounds and between Nd and Sm for the Ba compounds [18].

Note that no ternary compounds of the lighter lanthanides (La–Nd) could be obtained either by stoichiometric reactions or with the aid of a flux. We do not know if such compounds are stable, and, if they are, what structure types they will adopt. It has been proposed [30] that when the radius of M^{2+} is larger than the radius of Ln^{3+} then the MLn_2O_4 compounds will crystallize in the calcium ferrite structure type. However, radius-ratio rules are of limited use for the chalcogenides, because they rely on a hard-sphere approximation that is not reliable when covalent bonding is involved. The role that the size of the Q^{2-} anion plays in determining structure type remains unknown.

Plots illustrating the trends of the cell constants versus the ionic radius of the rare-earth atom are shown in Fig. 3. These cell constants decrease linearly with decreasing radius. Because the changes in cell constants are small, the volume of the cell also decreases linearly with decreasing radius. Although the values used for ionic radii are the usual ones [31], the anomalies at Y suggest that its ionic radius falls between those of Dy and Ho for these tellurides. This has also been noted previously with the sulfides [15] and selenides [2] of this family.

In addition to the decrease of the cell parameters, the overall distortion in the structure decreases with decreasing ionic radius. This distortion is present to some extent in all compounds that possess the calcium ferrite structure type.

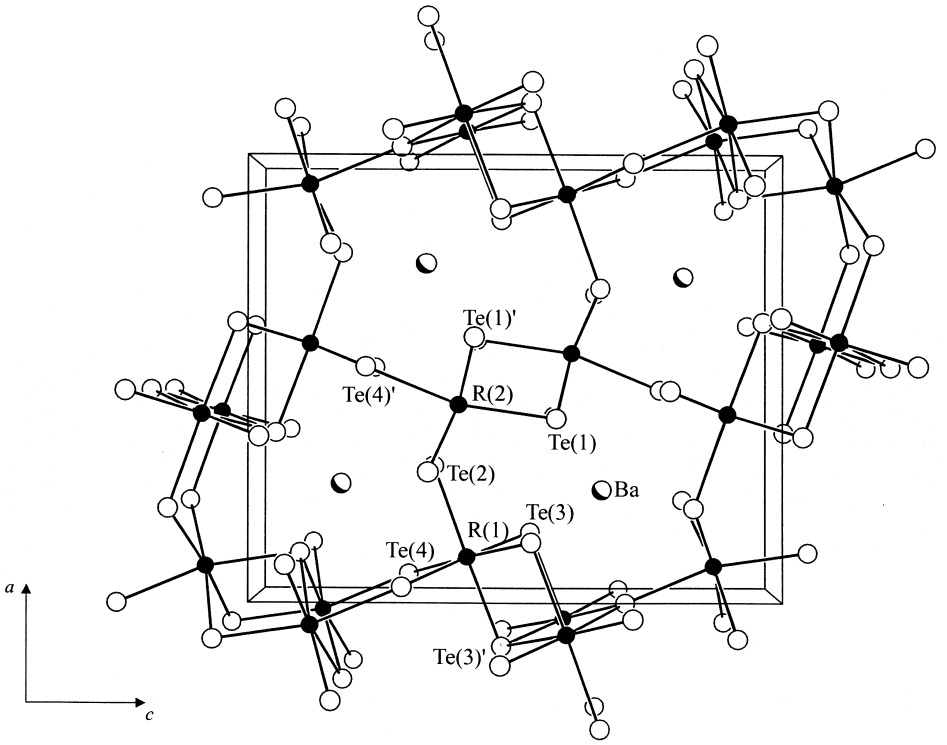

Fig. 1. View down [010] of the unit cell of $BaLn_2Te_4$ showing the three-dimensional channel structure. Here and in subsequent figures atoms are of arbitrary size.

Why exactly the distortion of one octahedral site is more pronounced than that of the other has never been adequately discussed. As a measure of the effect of the size of the Ln^{3+} cation on the distortion in the present compounds, the shift of each Ln atom out of the equatorial plane of its respective octahedron, formed by atoms Te(3) and Te(4)

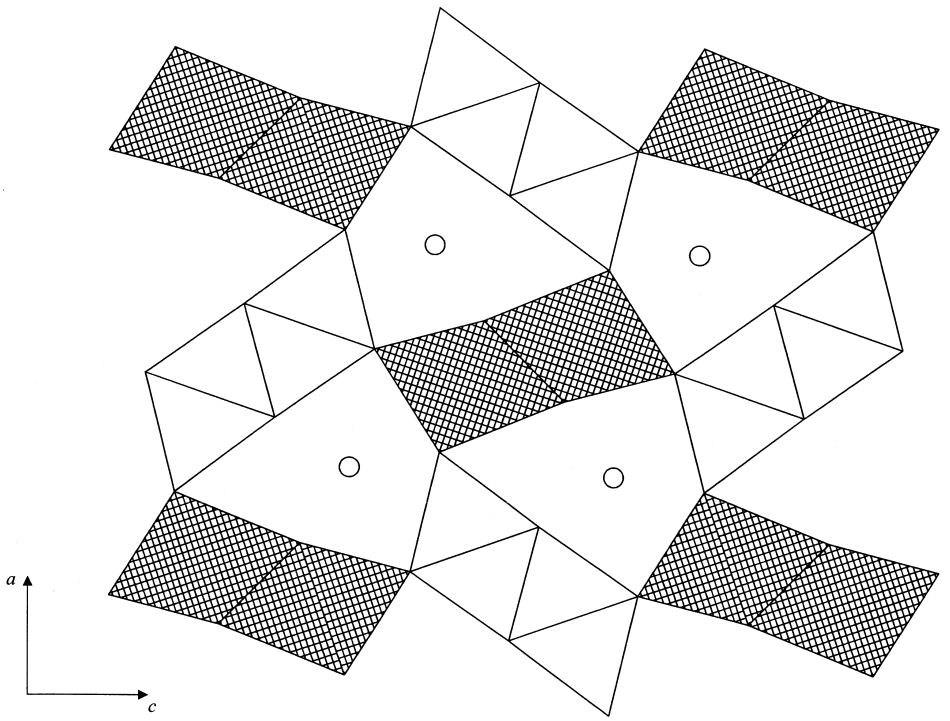

Fig. 2. Polyhedral view down [010] of $BaLn_2Te_4$. Light polyhedra are Ln(1)-centered, dark polyhedra are Ln(2)-centered. Open circles are Ba atoms.

Table 3
Selected bond lengths (Å) for $BaLn_2Te_4$

Ln=	Sm	Gd	Tb	Dy	Y	Ho	Er	Tm
Ln(1)–Te(4)×2	3.0756(5)	3.0593(4)	3.0424(9)	3.0383(7)	3.0345(12)	3.0258(5)	3.0154(8)	3.0057(6)
Ln(1)–Te(3)	3.1124(7)	3.0889(6)	3.0714(14)	3.0593(11)	3.0574(19)	3.0454(8)	3.0355(11)	3.0223(8)
Ln(1)–Te(3)×2	3.1303(5)	3.1047(4)	3.0878(9)	3.0774(8)	3.0732(12)	3.0628(5)	3.0512(8)	3.0388(6)
Ln(1)–Te(2)	3.1388(7)	3.1247(6)	3.1099(14)	3.1028(11)	3.1032(19)	3.0923(8)	3.0832(11)	3.0715(9)
Ln(2)–Te(1)	3.0828(7)	3.0633(6)	3.0434(13)	3.0343(11)	3.0343(18)	3.0230(8)	3.0115(11)	2.9987(8)
Ln(2)–Te(4)	3.1100(7)	3.0868(6)	3.0719(13)	3.0595(11)	3.0544(18)	3.0489(8)	3.0393(11)	3.0291(8)
Ln(2)–Te(1)×2	3.1235(5)	3.1038(4)	3.0857(10)	3.0789(8)	3.0741(13)	3.0640(5)	3.0524(8)	3.0428(6)
Ln(2)–Te(2)×2	3.1368(5)	3.1205(4)	3.1053(10)	3.0995(8)	3.0944(13)	3.0860(5)	3.0755(8)	3.0653(6)
Ba(1)–Te(3)×2	3.5370(6)	3.5269(5)	3.5183(11)	3.5174(9)	3.5125(11)	3.5093(7)	3.5042(10)	3.5016(7)
Ba(1)–Te(1)×2	3.5477(6)	3.5481(5)	3.5435(11)	3.5455(9)	3.5406(11)	3.5392(7)	3.5347(10)	3.5307(7)
Ba(1)–Te(2)×2	3.5416(6)	3.5472(5)	3.5483(11)	3.5515(9)	3.5514(11)	3.5491(7)	3.5499(9)	3.5478(7)
Ba(1)–Te(4)	3.7094(8)	3.7128(6)	3.7049(16)	3.6991(12)	3.6925(15)	3.6880(9)	3.6757(13)	3.6658(10)
Ba(1)–Te(4)	3.7479(8)	3.7250(6)	4.3455(13)	3.7057(13)	3.7073(16)	3.6944(9)	3.6916(13)	3.6816(10)

for Ln(1), and atoms Te(1) and Te(2) for Ln(2), is shown as a function of ionic radius (Fig. 4). An interesting trend is observed. The shift of Ln(2) decreases dramatically with decreasing size of the rare-earth atom but the shift of Ln(1) tends to increase slightly. This can be rationalized by considering the Ln_2Te_4 framework to be a flexible network of Ln-centered octahedra. Thus as the size of the Ln atom increases, the Ln(2) atoms are shifted farther away from the centers of their octahedra and the Ln(1) atoms are subsequently pulled into a more regular environment.

Initially, the dependence of molar magnetic susceptibility on temperature was fit by least-squares methods to the modified Curie–Weiss relation $\chi=\chi_o+C/(T+\theta)$, but the resultant values of χ_o were not significantly different from zero. Thus, the Curie–Weiss law was used. Plots of χ^{-1} vs. T for the Er and Tm compounds are shown in Fig. 5 and values for θ and C as well as the effective magnetic moment, $\mu_{eff}=\sqrt{8C}\ \mu_B$ where μ_B is the Bohr magneton, are given in Table 5. The value of μ_{eff} of 8.9(1) μ_B for Er^{3+} may be compared with 9.07 μ_B for Er_2Te_3 [32], 10.3 μ_B for $ErGe_{1.83}$ [33], and the 'average' experimental value of 9.5 μ_B [34]. The value of μ_{eff} of 7.3(3) μ_B for Tm^{3+} agrees with the 'average' experimental value of 7.3 μ_B [34].

Acknowledgements

This research was supported by NSF Grant No. DMR-9709351. A.B. Sipes was funded by NSF Grant No. DMR-9803995 (NSF Summer Research Program in Solid State Chemistry) and M.A. Digman by NSF-MRL Grant

Table 4
Selected angles (°) in $BaLn_2Te_4$

Ln=	Sm	Gd	Tb	Dy	Y	Ho	Er	Tm
Te(4)–Ln(1)–Te(3)×2	90.02(2)	86.66(1)	86.56(2)	86.52(2)	86.60(2)	86.51(1)	86.47(2)	86.35(1)
Te(3)–Ln(1)–Te(3)×2	88.40(2)	88.10(1)	87.87(3)	87.72(2)	87.69(4)	87.62(2)	87.51(3)	87.32(2)
Te(4)–Ln(1)–Te(3)×2	86.61(1)	89.87(1)	89.91(3)	89.93(2)	89.94(4)	89.96(2)	90.01(3)	90.08(2)
Te(4)–Ln(1)–Te(2)×2	89.96(2)	90.34(1)	90.68(3)	90.80(2)	90.78(4)	90.98(2)	91.17(3)	91.23(2)
Te(3)–Ln(1)–Te(2)×2	91.62(2)	91.70(1)	91.53(3)	91.53(2)	91.58(4)	91.43(2)	91.30(3)	91.36(2)
Te(3)–Ln(1)–Te(3)	92.30(2)	92.41(1)	92.50(3)	92.65(3)	92.58(5)	92.70(2)	92.76(3)	92.92(2)
Te(4)–Ln(1)–Te(4)	94.44(2)	94.20(2)	94.30(4)	94.21(3)	94.12(5)	94.18(2)	94.20(3)	94.26(2)
Te(4)–Ln(1)–Te(3)×2	178.11(2)	177.79(2)	177.62(4)	177.55(3)	177.52(6)	177.48(2)	177.43(3)	177.33(3)
Te(3)–Ln(1)–Te(2)	179.97(2)	179.70(2)	179.12(4)	178.92(3)	178.94(6)	178.62(2)	178.28(3)	177.89(2)
Te(4)–Ln(2)–Te(1)×2	82.84(2)	83.52(1)	83.78(3)	84.06(2)	84.25(4)	84.29(2)	84.44(2)	84.59(2)
Te(1)–Ln(2)–Te(1)×2	85.21(2)	85.66(1)	85.73(3)	85.69(2)	85.70(4)	85.67(2)	85.65(2)	85.56(2)
Te(1)–Ln(2)–Te(2)×2	86.84(1)	87.32(1)	87.36(2)	87.46(2)	87.53(2)	87.49(1)	87.50(2)	87.48(1)
Te(4)–Ln(2)–Te(2)×2	87.26(2)	88.58(1)	89.16(3)	89.70(2)	89.81(4)	90.02(2)	90.40(2)	90.68(2)
Te(2)–Ln(2)–Te(2)	92.05(2)	91.81(2)	91.83(4)	91.80(3)	91.76(5)	91.80(2)	91.81(3)	91.89(2)
Te(1)–Ln(2)–Te(1)	92.56(2)	92.45(2)	92.58(4)	92.59(3)	92.55(5)	92.65(2)	92.71(3)	92.77(2)
Te(1)–Ln(2)–Te(2)×2	104.59(2)	102.22(1)	101.34(3)	100.58(2)	100.26(4)	100.06(2)	99.55(2)	99.22(2)
Te(1)–Ln(2)–Te(4)	162.67(2)	164.33(2)	164.80(4)	165.14(3)	165.45(6)	165.44(2)	165.63(3)	165.70(3)
Te(1)–Ln(2)–Te(2)×2	170.08(2)	172.07(2)	172.91(4)	173.71(3)	174.03(6)	174.26(2)	174.79(3)	175.22(2)

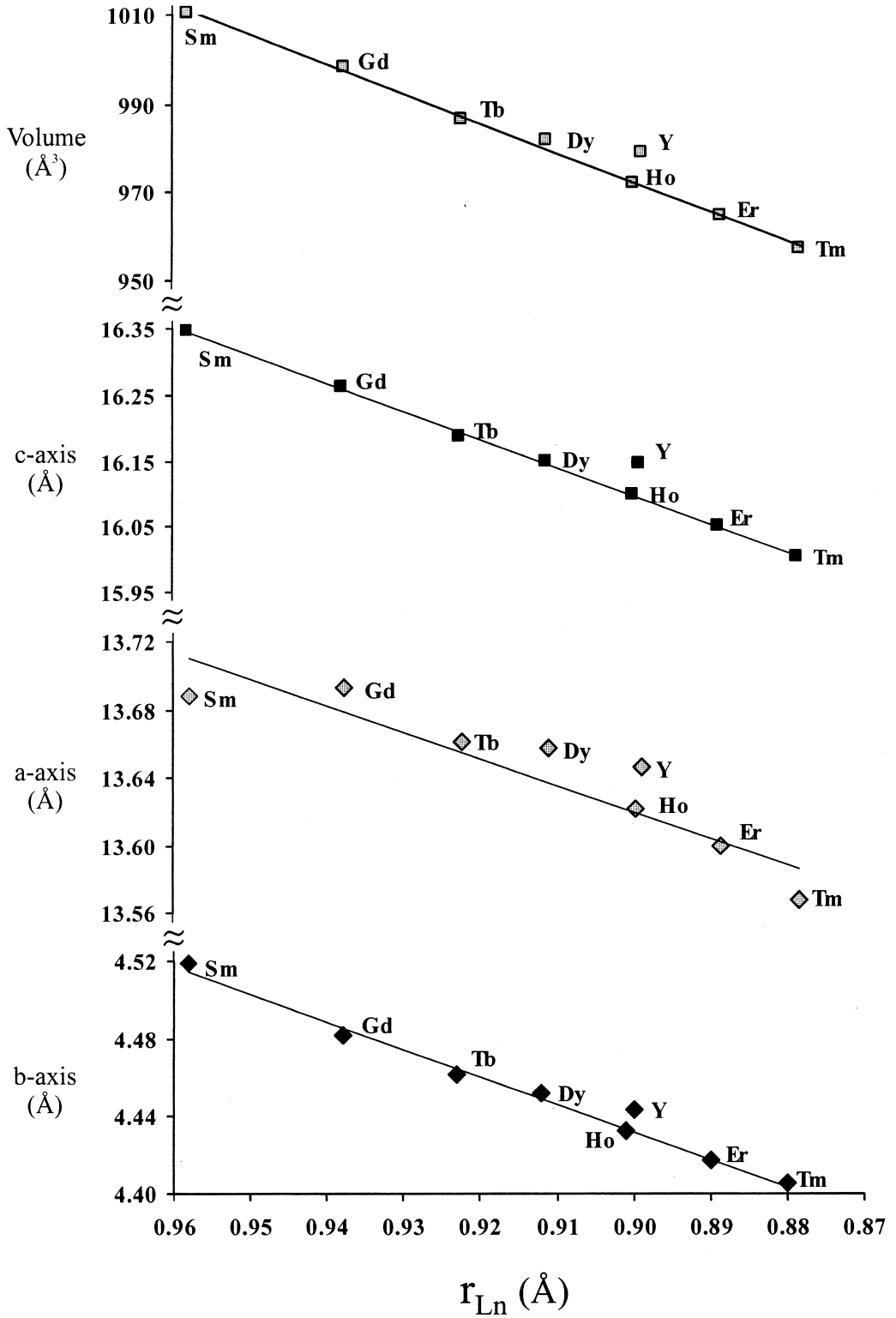

Fig. 3. Plots of axis length versus ionic radius for all $BaLn_2Te_4$ compounds. The lines represent the best linear fit to the data, excluding Y in all cases. No error bars are given, as the errors in cell constants, though undoubtedly larger than those stated in Table 1, remain small compared with the scale of the ordinate.

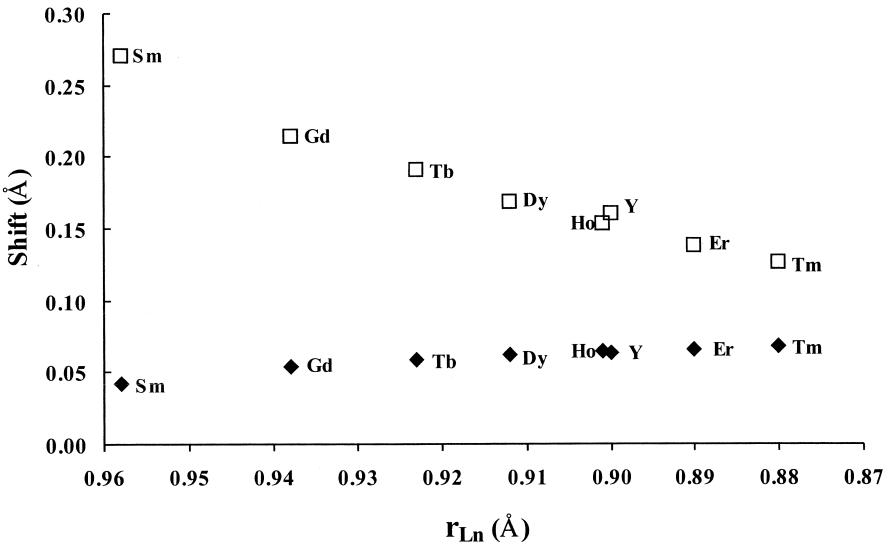

Fig. 4. Plot showing the shift out of the equatorial plane versus ionic radius for the two independent Ln atoms. ♦, Ln(1); and □, Ln(2).

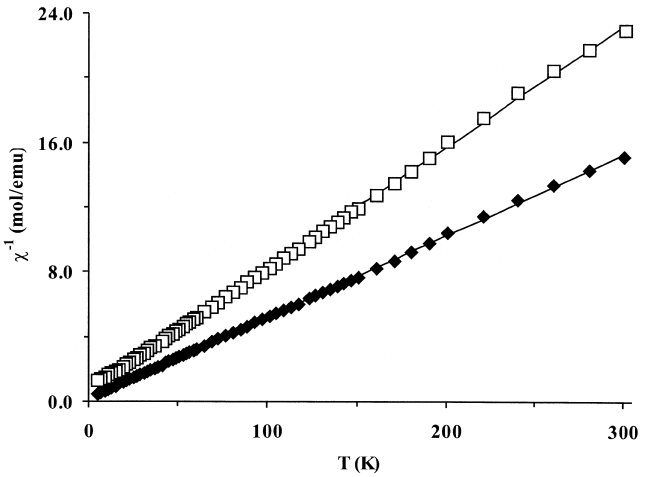

Fig. 5. Plots of inverse magnetic susceptibility versus temperature for $BaEr_2Te_4$ (♦) and $BaTm_2Te_4$ (□). The lines represent the least-squares fit to the Curie–Weiss relation.

No. DMR-9120521. This work made use of Central Facilities supported by the MRSEC program of the National Science Foundation (DMR-9632472) at the Materials Research Center of Northwestern University. We are indebted to M.Z. Lin for his assistance with the magnetic susceptibility measurements and to Dr. Olivier Tougait for his assistance with the synthesis of $BaGd_2Te_4$.

Table 5
Magnetic properties for Ln=Er and Tm

	θ (K)	C (emu K/mol)	μ_{eff} (μ_B)
$BaEr_2Te_4$	3.85(6)	9.95(5)	8.9(1)
$BaTm_2Te_4$	9.15(3)	6.65(15)	7.3(3)

References

[1] J. Flahaut, L. Domange, M. Patrie, Bull. Soc. Chim. Fr. (1962) 159–163.
[2] J. Dugué, D. Carré, M. Guittard, Acta Crystallogr., Sect. B: Struct. Crystallogr. Cryst. Chem. 34 (1978) 3564–3568.
[3] A.F. Reid, J. Am. Ceram. Soc. 50 (1967) 491–492.
[4] T.L. Barry, R. Roy, J. Inorg. Nucl. Chem. 29 (1968) 1243–1248.
[5] E. Paletta, H. Müller-Buschbaum, J. Inorg. Nucl. Chem. 30 (1968) 1425–1432.
[6] H. Müller-Buschbaum, Z. Anorg. Allg. Chem. 358 (1968) 138–146.
[7] M.-P. Pardo, J. Flahaut, Bull. Soc. Chim. Fr. (1969) 6–9.
[8] N. Rodier, V. Tien, C.R. Séances Acad. Sci., Ser. C 284 (1977) 909–911.
[9] K.R. Bkhargava, L.M. Kovba, L.I. Martynenko, V.I. Spitsyn, Dokl. Chem. (Engl. Trans.) 161 (1965) 294–296.
[10] G.A. Costa, M. Ferretti, M.L. Fornasini, E.A. Franceschi, G.L. Olcese, Powder Diffract. 4 (1989) 24–25.
[11] W. Wong-Ng, B. Paretzkin, Powder Diffract. 6 (1991) 187–189.
[12] J.D. Carpenter, S.-J. Hwu, J. Solid State Chem. 97 (1992) 332–339.
[13] J.D. Carpenter, S.-J. Hwu, Acta Crystallogr., Sect. C: Cryst. Struct. Commun. 48 (1992) 1164–1167.
[14] C. Cascales, I. Rasines, Powder Difract. 10 (1995) 122–126.
[15] C.K. Lowe-Ma, T.A. Vanderah, T.E. Smith, J. Solid State Chem. 117 (1995) 363–372.
[16] J. Flahaut, in: K.A. Gschneidner Jr., L.R. Eyring (Eds.), Handbook on the Physics and Chemistry of Rare Earths, Vol. 4, Amsterdam, New York, 1979, pp. 1–88.
[17] S.M. Golabi, J. Flahaut, L. Domange, C.R. Acad. Sci. Paris 259 (1964) 820–822.
[18] A.A. Eliseev, G.M. Kuzmichyeva, in: K.A. Gschneidner Jr., L.R. Eyring (Eds.), Handbook on the Physics and Chemistry of Rare Earths, Vol. 13, North-Holland, New York, 1990, pp. 191–280.
[19] M. Patrie, J. Flahaut, C.R. Acad. Sci. Paris 264 (1967) 395–398.
[20] H.L. Tsai, P.J. Meschter, J. Electrochem. Soc. 128 (1981) 2229–2232.
[21] C.O. Diaz, B.G. Hyde, Acta Crystallogr., Sect. B: Struct. Sci. 39 (1983) 569–575.
[22] J.C. Huffman, Ph.D. thesis, Indiana University, 1974.
[23] SMART Version 5.05A and SAINT Plus Version 6.0 Data Collection and Processing Software for the SMART System. Bruker Analytical X-Ray Instruments, Inc., Madison, WI, USA.

[24] G.M. Sheldrick SHELXTL DOS/Windows/NT Version 5.10. Bruker Analytical X-Ray Instruments, Inc., Madison, WI, USA.
[25] G.M. Sheldrick, Acta Crystallogr., Sect. A: Cryst. Phys., Diffr., Theor. Gen. Crystallogr. 46 (1990) 467–473.
[26] L.N. Mulay, E.A. Boudreaux (Eds.), Theory and Applications of Molecular Diamagnetism, Wiley-Interscience, New York, 1976.
[27] J.S. Swinnea, H. Steinfink, L.R. Danielson, J. Appl. Crystallogr. 20 (1987) 102–104.
[28] G. Ghémard, J. Etienne, G. Schiffmacher, J. Flahaut, J. Solid State Chem. 45 (1982) 146–153.
[29] B.F. Decker, J.S. Kasper, Acta Crystallogr. 10 (1957) 332–337.
[30] H.K. Müller-Buschbaum, R. von Schenck, Z. Anorg. Allg. Chem. 377 (1970) 70–78.
[31] R.D. Shannon, Acta Crystallogr., Sect. A: Cryst. Phys., Diffr., Theor. Gen. Crystallogr. 32 (1976) 751–767.
[32] K. Stowe, Z. Anorg. Allg. Chem. 624 (1998) 872–876.
[33] O. Oleksyn, P. Schobinger-Papamantellos, C. Ritter, C.H. de Groot, K.H.J. Buschow, J. Alloys Comp. 252 (1997) 53–58.
[34] C. Kittel, Introduction to Solid State Physics, 6th Edition, Wiley, New York, 1986.